Inorg. Chem. **2007**, *46*, 7848–7860

Seven-Coordinate Iron Complex as a Ditopic Receptor for Lithium Salts: Study of Host–Guest Interactions and Substitution Behavior

David Sarauli,[†] Vesselina Popova,[‡] Achim Zahl,[†] Ralph Puchta,[†] and Ivana Ivanović-Burmazović*[,†]

Institute for Inorganic Chemistry, University of Erlangen-Nürnberg, Egerlandstrasse 1, D-91058 Erlangen, Germany, Max-Planck-Institute for Iron Research GmbH, Max-Planck-Strasse 1, D-40237 Düsseldorf, Germany

Received March 15, 2007

Interactions between the seven-coordinate tweezerlike $[Fe(dapsox)(H_2O)_2]ClO_4$ complex (H_2dapsox = 2,6-diacetylpyridine-bis(semioxamazide)) with different lithium salts (LiOTf, $LiClO_4$, $LiBF_4$, and $LiPF_6$) in CH_3CN have been investigated by electrochemical, spectrophotometric, ^{7}Li and ^{19}F NMR, kinetic, and DFT methods. It has been demonstrated that this complex acts as ditopic receptor, showing spectral and electrochemical ion-pair-sensing capability for different lithium salts. In general, the apparent binding constants for lithium salts increase in the order LiOTf < $LiClO_4$ < $LiBF_4$. From the electrochemical measurements, the apparent lithium salt binding constants for the Fe(III) and Fe(II) forms of the complex have been obtained, suggesting a stronger host–guest interaction with the reduced form of the complex. In the presence of $LiPF_6$, the solution chemistry is more complex because of the hydrolysis of PF_6^-. The kinetics of the complexation of $[Fe(dapsox)(CH_3CN)_2]^+$ by thiocyanate at –15 °C in acetonitrile in the presence of 0.2 M NBu_4OTf shows two steps with the following rate constants and activation parameters: $k_1 = 411 \pm 14$ M^{-1} s^{-1}; $\Delta H_1^{\neq} = 9 \pm 2$ kJ mol^{-1}; $\Delta S_1^{\neq} = -159 \pm 6$ J K^{-1} mol^{-1}; $k_2 = 52 \pm 1$ M^{-1} s^{-1}; $\Delta H_2^{\neq} = 4 \pm 1$ kJ mol^{-1}; $\Delta S_2^{\neq} = -195 \pm 3$ J K^{-1} mol^{-1}. The very negative $\Delta S^{\neq}$ values are consistent with an associative (A) mechanism. Under the same conditions but with 0.2 M LiOTf, k_{1Li} and k_{2Li} are 1605 ± 51 and 106 ± 2 M^{-1} s^{-1}, respectively. The increased rate constants for the $\{[Fe(dapsox)(CH_3CN)_2]\cdot LiOTf\}^+$ adduct are in agreement with an associative mechanism. Kinetic and spectrophotometric titration measurements show stronger interaction between the lithium salt and the anion-substituted forms, $[Fe(dapsox)(CH_3CN)(NCS)]$ and $[Fe(dapsox)(NCS)_2]^-$, of the complex. These experiments demonstrate that in nonaqueous media lithium salts cannot be simply used as supporting electrolytes, since they can affect the kinetic behavior of the studied complex. DFT calculations revealed that the negatively charged α-oxyazine oxygen atoms are responsible for cation binding (electrostatic interactions), whereas the two terminal amide groups bind the anion via hydrogen bonding.

Introduction

The solution properties and mechanistic behavior of seven-coordinate 3d metal complexes are still unrevealed research areas. These complexes are especially interesting as excellent low-molecular-weight catalysts for superoxide ($O_2^{\bullet -}$) dismutation (SOD), providing important therapeutic applications.[1] Although the best SOD mimetics known to date are seven-coordinate complexes of Mn(II) with macrocyclic pentadentate ligands, iron SOD mimetics would also be desirable because of their higher kinetic and thermodynamic stability than manganese complexes.[2]

To gain an understanding of the solution chemistry of the iron seven-coordinate complexes, the substitution behavior and proton-coupled electron-transfer reactions of the pentagonal-bypiramidal (PBP) Fe(III) complex, $[Fe(dapsox)(H_2O)_2]^+$ (H_2dapsox = 2,6-diacetylpyridine-bis(semioxamazide)),[3] with an anionic planar pentadentate ligand in the

* To whom correspondence should be addressed. E-mail: Ivana.Ivanovic@chemie.uni-erlangen.de.
[†] Institute for Inorganic Chemistry.
[‡] Max-Planck-Institute for Iron Research GmbH.

(1) (a) Aston, K.; Rath, N.; Naik, A.; Slomczynska, U.; Schall, O. F.; Riley, D. P. *Inorg. Chem.* **2001**, *40*, 1779−1789. (b) Salvemini, D.; Riley, D. P.; Cuzzocrea, S. *Nat. Rev. Drug Discovery* **2002**, *1*, 367−374. (c) Muscoli, C.; Cuzzocrea, S.; Riley, D. P.; Zweier, J. L.; Thiemermann, C.; Wang, Z.-Q.; Salvemini, D. *Br. J. Pharmacol.* **2003**, *140*, 445−460.
(2) Riley, D. P. *Chem. Rev.* **1999**, *99*, 2573−2587.

10.1021/ic7005056 CCC: $37.00
Published on Web 08/23/2007

Scheme 1

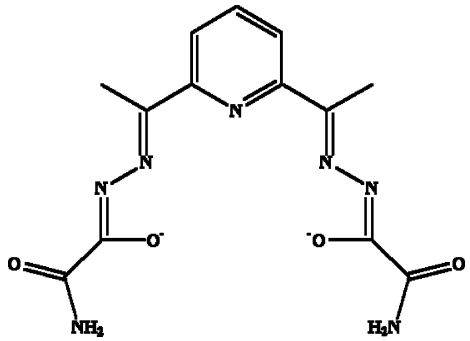

equatorial plane (Scheme 1), were systematically studied.[4] Mechanistic information on the two-step displacement of the trans-coordinated solvent molecules by the monodentate monoanionic thiocyanate ligand were obtained in the case of H_2O, MeOH, EtOH, and DMSO as axial ligands.[4b,c] The latter solvent was selected because kinetic experiments with the superoxide radical anion, especially with more concentrated solutions (in the millimolar range), require the use of aprotic solvents and the mixing of potassium superoxide solutions with aqueous or alcoholic solutions of the studied complexes for the kinetic measurements at ambient and low temperatures, respectively. In the DMSO/CH_3CN (29:71) mixture, it is possible to perform low-temperature kinetic measurements down to −53 °C.[5] In this respect, it was important to understand the substitution behavior of [Fe(dapsox)$(H_2O)_2$]ClO_4 in the CH_3CN solution as well.

In general, kinetic measurements should be performed at constant ionic strength, requiring the use of so-called "innocent" salts as supporting electrolytes, which do not coordinate to the metal center in solution. Because of the good solubility, tetraalkylammonium and some lithium salts are suitable as supporting electrolytes in aprotic solvents like DMSO and CH_3CN. However, added salts can exert strong effects on the rates of reactions between charged species in solution, affecting solvation of inorganic complexes.[6] The interaction via hydrogen bonds should also be taken into consideration, especially in aprotic solvents where these interactions are more prominent.[7] The electrostatic interactions and hydrogen-bonding also play an important role in the host−guest chemistry, in designing specific receptors for small ions, and in generating a dynamic combinatorial library (DCL) as a new strategy for identifying receptors of high affinity for the respective target.[8] Amide-group-containing receptors are very often used for anion recognition,[9] whereas hydrazone chemistry was involved in creating DCLs and the discovery of receptors for cations, like ammonium,[10] cobalt(II),[11] and Li^+.[12] Receptors for Li^+ are of special interest since Li^+ is the smallest metal cation and has clinical, pharmacological, and biochemical importance.[13]

In light of the above-mentioned aspects, it was of importance to investigate whether the nature of added electrolyte can exert a significant effect on substitution kinetics of our seven-coordinate Fe(III) complex in CH_3CN solution, especially due to the fact that our dapsox^{2-} ligand possesses two amide and two hydrazone functional groups at the same time. Thus, from a structural point of view, our seven-coordinate iron complex can potentially be a ditopic receptor, capable of binding anions and small cations simultaneously.

Herein we report the results from electrochemical, ^{7}Li and ^{19}F NMR, and DFT studies of the host−guest interactions between the seven-coordinate [Fe(dapsox)$(CH_3CN)_2$]$^+$ complex and different lithium salts in CH_3CN. The kinetic and spectrophotometric studies on the substitution behavior of this PBP iron(III) complex in the presence and absence of lithium ions in acetonitrile solutions have also been reported. Since the seven-coordinate pentagonal-bipyramidal 3d metal complexes with planar pentadentate ligands are known to be synthetic SOD enzymes,[1] simulation of an enzymatic active site, which could bind small metal cations and in that way enhance binding of superoxide, would be of importance.

Experimental Section

Materials. The solvents acetonitrile (Roth, dry, ≥99.9%, ≤0.001% H_2O), DMSO (Acros Organics, ≥99.9%, ≤0.1% H_2O), and methanol (Roth, ≥99.9%, ≤0.005% H_2O), as well as the salts NaSCN (Aldrich, 96%), LiOTf (Aldrich, 96%), $LiClO_4$ (Aldrich, 98%), $LiBF_4$ (Aldrich, 98%), $LiPF_6$ (Acros Organics, 98%), $NaClO_4$

(3) Andjelkovic, K.; Bacchi, A.; Pelizzi, G.; Jeremic, D.; Ivanović-Burmazović, I. *J. Coord. Chem.* **2002**, *55*, 1385−1392.

(4) (a) Sarauli, D.; Meier, R.; Liu, G.-F.; Ivanović-Burmazović, I.; van Eldik, R. *Inorg. Chem.* **2005**, *44*, 7624−7633. (b) Ivanović-Burmazović, I.; Hamza, M. S. A.; van Eldik, R. *Inorg. Chem.* **2002**, *41*, 5150−5161. (c) Ivanović-Burmazović, I.; Hamza, M. S. A.; van Eldik, R. *Inorg. Chem.* **2006**, *45*, 1575−1584.

(5) (a) McClune, G. J. *Iron catalyzed superoxide dismutation*; University of Michigan: Ann Arbor, MI, 1979, From: *Diss. Abstr. Int. B 40*, 2175. (b) Dürr, K.; Macpherson, B. P.; Warratz, R.; Hampel, F.; Tuczek, F.; Helmreich, M.; Jux, N.; Ivanović-Burmazović, I. *J. Am. Chem. Soc.* **2007**, *129*, 4217−4228.

(6) (a) Grigoriev, V. A.; Cheng, D.; Hill, C. L.; Weinstock, I. A. *J. Am. Chem. Soc.* **2001**, *123*, 5292−5307. (b) Curtis, J. C.; Inagaki, M.; Chun, S. J.; Eskandari, V.; Luo, X.; Pan, Z. N.; Sankararaman, U.; Pengra, G. E.; Zhou, J.; Hailey, P.; Laurent, J.; Utalan, D. *Chem. Phys.* **2006**, *326*, 43−53.

(7) (a) Beer, P. D.; Gale, P. A. *Angew. Chem., Int. Ed.* **2001**, *40*, 486−516. (b) Bu, J.; Lilienthal, N. D.; Woods, J. E.; Nohrden, C. E.; Hoang, K. T.; Truong, D.; Smith, D. K. *J. Am. Chem. Soc.* **2005**, *127*, 6423−6429. (c) Prins, L. J.; Reinhoudt, D. N.; Timmerman, P. *Angew. Chem., Int. Ed.* **2001**, *40*, 2382−2426. (d) Rudner, M. S.; Jeremic, S.; Petterson, K. A.; Kent, D. R.; Brown, K. A.; Drake, M. D.; Goddard, W. A., III; Roberts, J. D. *J. Phys. Chem. A* **2005**, *109*, 9076−9082.

(8) Corbett, P. T.; Leclaire, J.; Vial, L.; West, K. R.; Wietor, J.-L.; Sanders, J. K. M.; Otto, S. *Chem. Rev.* **2006**, *106*, 3652−3711.

(9) (a) Evans, A. J.; Beer, P. D. *Dalton Trans.* **2003**, 4451−4456. (b) Mahoney, J. M.; Beatty, A. M.; Smith, B. D. *Inorg. Chem.* **2004**, *43*, 7617−7621. (c) Mahoney, J. M.; Stucker, K. A.; Jiang, H.; Carmichael, I.; Brinkmann, N. R.; Beatty, A. M.; Noll, B. C.; Smith, B. D. *J. Am. Chem. Soc.* **2005**, *127*, 2922−2928. (d) Lankshear, M. D.; Cowley, A. R.; Beer, P. D. *Chem. Comm.* **2006**, 612−614.

(10) Cousins, G. R. L.; Furlan, R. L. E.; Ng, Y.-F.; Redman, J. E.; Sanders, J. K. M. *Angew. Chem., Int. Ed.* **2001**, *40*, 423−428.

(11) Guo, D.; Han, G.; Duan, C.-y.; Pang, K.-l.; Meng, Q.-j. *Chem. Comm.* **2002**, 1096−1097.

(12) Furlan, R. L. E.; Ng, Y.-F.; Otto, S.; Sanders, J. K. M. *J. Am. Chem. Soc.* **2001**, *123*, 8876−8877.

(13) (a) Christian, G. D. *Sensors* **2002**, *2*, 432−435. (b) Christian, G. D. *J. Pharm. Biomed. Anal.* **1996**, *14*, 899−908. (c) Srinivasan, C.; Toon, J.; Amari, L.; Abukhdeir, A. M.; Hamm, H.; Geraldes, C. F. G. C.; Ho, Y.-K.; Mota de Freitas, D. *J. Inorg. Biochem.* **2004**, *98*, 691−701. (d) Layden, B. T.; Abukhdeir, A. M.; Malarkey, C.; Oriti, L. A.; Salah, W.; Stigler, C.; Geraldes, C. F. G. C.; Mota de Freitas, D. *Biochim. Biophys. Acta* **2005**, *1741*, 339−349. (e) Sastre, E.; Nicolay, A.; Bruguerolle, B.; Portugal, H. *Life Sci.* **2005**, *77*, 758−767. (f) Parker, M. S.; Parker, S. L.; Kane, J. K. *Regul. Pept.* **2004**, *118*, 67−74.

(Acros Organics, 99+%), and all tetrabutylammonium (TBA) salts (Fluka, ≥99%, puriss electrochemical grade) were used as received without further purification. The water content in solutions was determined by Karl Fischer titrations. $[Fe(dapsox)(H_2O)_2]ClO_4$ was prepared and characterized previously.[3,14] The $[Fe(dapsox)(NCS)_2]^-$ species was prepared in situ by adding a minimum 100-fold excess of NaSCN to the acetonitrile solution of $[Fe(dapsox)(H_2O)_2]ClO_4$.

Kinetic Measurements. All data were obtained by recording time-resolved UV/vis spectra using a modified Bio-Logic stopped-flow module μSFM-20 combined with a Huber CC90 thermostat (±0.1°) and equipped with a J & M TIDAS high-speed diode-array spectrometer with combined deuterium and tungsten lamps (200−1015 nm wavelength range). Data were analyzed using the integrated Bio-Kine software, version 4.23, and the Specfit/32 program. At least 10 kinetic runs were recorded under all conditions, and the reported rate constants represent the mean values. All kinetic measurements were carried out under pseudo-first-order conditions, i.e., the substituent concentration was in a large excess (concentrations of iron complex were 5×10^{-5} M). The reactions were studied at a constant ionic strength (0.2 M). Values of $\Delta H^{\neq}$ and $\Delta S^{\neq}$ were calculated from the slopes and intercepts of plots of $\ln(k/T)$ vs $1/T$, respectively.

Spectrophotometric Titrations. UV/vis spectra were recorded on a Hewlett-Packard 8542A spectrophotometer at 25 °C. Solutions of $[Fe(dapsox)(CH_3CN)_2]^+$ and $[Fe(dapsox)(NCS)_2]^-$ (5×10^{-5} and 1×10^{-4} M) in acetonitrile were placed in a 1.0 cm path length cuvette in the thermostated cell block of a spectrophotometer for 10−15 min. These solutions were titrated by the addition of small aliquots of concentrated stock solutions of substrates (NaSCN, LiOTf, $LiBF_4$, and $LiPF_6$) in CH_3CN. The spectra were recorded after equilibration for 10 min.

Electrochemical Measurements. Cyclic (CV) and differential pulse (DPV) voltammetry measurements were performed with an Autolab PGSTAT 30 device (Eco Chemie). All measurements were conducted under N_2 in a jacketed, one-compartment cell with the Au disk working electrode (geometric area: 0.07 cm^2) (Metrohm), a platinum wire counter electrode (Metrohm), and a Ag wire pseudo-reference electrode. The working electrode surface was polished with 0.05-μm alumina, sonicated in water, and air-dried immediately before use. Various NBu_4A ($A = PF_6^-$, BF_4^-, ClO_4^-, OTf^-) salts (0.1 M) were used as electrolytes. The sweep rate was 50 mV/s. No IR compensation was applied. The stoichiometry of each electron-transfer was established by wave-height comparisons with known one-electron redox processes. O_2 was removed from the electrolyte solution by bubbling N_2 through the solvent for several minutes prior to making the measurement. A N_2 atmosphere was continuously maintained above the solution while the experiments were in progress. Temperature was controlled by using a circulating water bath to run 25 °C water through the outer cell jacket.

In order to improve solubility of the complex, solutions were prepared in dry CH_3CN containing a maximum of 0.1% DMSO. To determine the equilibrium associated with the redox-dependent binding, titration measurements were run in 0.1 M NBu_4A electrolyte solutions, using the seven-coordinate Fe(III) complex as the receptor and different lithium and/or tetrabutylammonium salts as the substrates. Experimentally, aliquots of concentrated lithium/tetrabutylammonium salt solutions were added incrementally to a 20 mL sample of the 1 mM iron complex, and cyclic voltammograms were run after each addition. Potentials are cited versus a Ag/AgCl electrode. The use of ferrocene as internal standard is not recommended, since its redox potential depends very much on the concentration of lithium salts present in the CH_3CN solution ($\Delta E = 30$ mV in the presence of 16 mM $LiBF_4$ and $\Delta E = 300$ mV in the presence of 16 mM $LiPF_6$, Figure S1).

Nuclear Magnetic Resonance Spectrometry. The ^{7}Li NMR measurements were conducted on a Bruker Avance DRX 400WB spectrometer using a 5 mm broadband probe. ^{19}F NMR spectra were recorded on a Bruker Avance DPX-300 spectrometer at 282.4 Hz. The solutions to be studied were placed in NMR tubes, and the solution of external standard (CF_2Br_2 in CD_3CN) in a concentric capillary was used for the field/frequency deuterium lock. All measurements were run at room temperature. The chemical shifts were related to CF_2Br_2 ($\delta_F = 7$ ppm vs $CFCl_3$). ^{7}Li NMR spectra were recorded at 155.5 MHz with a spectral width of 620 Hz and an acquisition time of 13 s. All systems were referenced to the free Li^+ salt (LiOTf) in DMF (external standard). Measurements were run at room temperature.

^{7}Li T_1 relaxation measurements were performed using the inversion recovery pulse sequence (D_1, 180°; τ, 90°). At least 15 τ values were used for each spin−lattice relaxation time (T_1) determination, and an interpulse delay of at least 10 times the T_1 value was used before repeating the pulse sequence. The observed T_1 values at different Li^+ concentrations were used to calculate the apparent binding constants K^{III} to the seven-coordinate $[Fe(dapsox)(CH_3CN)_2]^+$ complex. The relaxation measurements were accompanied by a 2−10% uncertainty.

Quantum Chemical Methods. We performed B3LYP/LANL2DZp hybrid density functional calculations, i.e., with pseudo-potentials on the heavy elements and the valence basis set augmented with polarization functions.[15] The resulting structures were characterized as minima by computation of vibrational frequencies, and the wave functions were tested for stability. The GAUSSIAN suite of programs was used.[16]

Results and Discussion

Electrochemical Studies. Cyclic voltammetry measurements of the seven-coordinate $[Fe(dapsox)(CH_3CN)_2]^+$ com-

(14) Ivanović-Burmazović, I.; Andjelkovic, K. *Adv. Inorg. Chem.* **2004**, *55*, 315−360.

(15) For recent papers that include the same type of calculations done, see: (a) Dees, A.; Zahl, A.; Puchta, R.; van Eikema Hommes, N. J. R.; Heinemann, F. W.; Ivanović-Burmazović, I. *Inorg. Chem.* **2007**, *46*, 2459−2470. (b) Summa, N.; Maigut, J.; Puchta, R.; van Eldik, R. *Inorg. Chem.* **2007**, *46*, 2094−2104. (c) Summa, N.; Schiessl, W.; Puchta, R.; van Eikema Hommes, N.; van Eldik, R. *Inorg. Chem.* **2006**, *45*, 2948−2959. (d) Puchta, R.; van Eikema Hommes, N.; Meier, R.; van Eldik, R. *Dalton Trans.* **2006**, 3392−3395. (e) Puchta, R.; Meier, R.; van Eikema Hommes, N. J. R.; van Eldik, R. *Eur. J. Inorg. Chem.* **2006**, 4063−4067. (f) Illner, P.; Zahl, A.; Puchta, R.; van Eikema Hommes, N.; Wasserscheid, P.; van Eldik, R. *J. Organomet. Chem.* **2005**, *690*, 3567−3576 and references therein.

(16) Frisch, M. J.; Trucks, G. W.; Schlegel, H. B.; Scuseria, G. E.; Robb, M. A.; Cheeseman, J. R.; Montgomery, J. A., Jr.; Vreven, T.; Kudin, K. N.; Burant, J. C.; Millam, J. M.; Iyengar, S. S.; Tomasi, J.; Barone, V.; Mennucci, B.; Cossi, M.; Scalmani, G.; Rega, N.; Petersson, G. A.; Nakatsuji, H.; Hada, M.; Ehara, M.; Toyota, K.; Fukuda, R.; Hasegawa, J.; Ishida, M.; Nakajima, T.; Honda, Y.; Kitao, O.; Nakai, H.; Klene, M.; Li, X.; Knox, J. E.; Hratchian, H. P.; Cross, J. B.; Bakken, V.; Adamo, C.; Jaramillo, J.; Gomperts, R.; Stratmann, R. E.; Yazyev, O.; Austin, A. J.; Cammi, R.; Pomelli, C.; Ochterski, J. W.; Ayala, P. Y.; Morokuma, K.; Voth, G. A.; Salvador, P.; Dannenberg, J. J.; Zakrzewski, V. G.; Dapprich, S.; Daniels, A. D.; Strain, M. C.; Farkas, O.; Malick, D. K.; Rabuck, A. D.; Raghavachari, K.; Foresman, J. B.; Ortiz, J. V.; Cui, Q.; Baboul, A. G.; Clifford, S.; Cioslowski, J.; Stefanov, B. B.; Liu, G.; Liashenko, A.; Piskorz, P.; Komaromi, I.; Martin, R. L.; Fox, D. J.; Keith, T.; Al-Laham, M. A.; Peng, C. Y.; Nanayakkara, A.; Challacombe, M.; Gill, P. M. W.; Johnson, B.; Chen, W.; Wong, M. W.; Gonzalez, C.; Pople, J. A. *Gaussian 03*, revision C.02; Gaussian, Inc.: Wallingford, CT, 2004.

Scheme 2

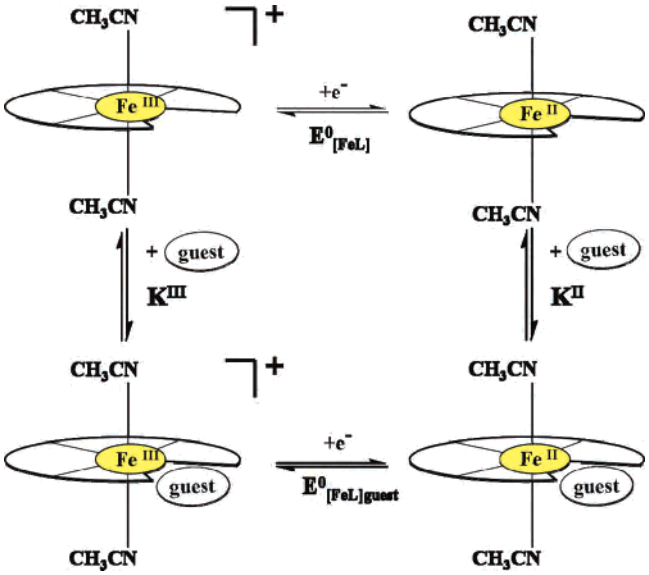

plex in the presence of different tetrabutylammonium (NBu_4^+) and lithium salts in CH_3CN afford a simple and effective way for estimating the communication between the redox-active iron center and binding sites for studied cation−anion pairs as potential guests. If present, an interaction between the seven-coordinate iron complex in both its oxidation states (Fe^{III} and Fe^{II}) and the ions in its substrate binding sites would result in a shift of the [Fe(dapsox)-$(CH_3CN)_2]^{0/+}$ couple redox potential upon increase of the salt concentration.[17] For the electrochemical guest binding titrations, the equilibria can be represented by a redox square (Scheme 2), and the interaction can be quantified by determining the apparent guest binding constant according to eq 1,[6a,17,18] where ΔE is a shift in the host redox potential as a function of guest concentration and K^{II} and K^{III} correspond to the 1:1 host/guest complex in the divalent and trivalent forms of the receptor, respectively.

$$\Delta E = \frac{RT}{F} \ln\left[\frac{1 + K^{II}[\text{guest}]}{1 + K^{III}[\text{guest}]}\right] \qquad (1)$$

However, no increase or decrease in the half-wave potential ($E_{1/2}$) of the $[Fe(dapsox)(CH_3CN)_2]^{0/+}$ couple (1 mM) was observed when concentrations of $NBu_4^+A^-$ ($A^- = PF_6^-$, BF_4^-, ClO_4^-, $CF_3SO_3^-$) were varied from 1 to 50 mM in the CH_3CN solution (Figure S2). Although in the crystal structure of $[Fe(dapsox)(H_2O)_2]ClO_4$ the charge-assisted hydrogen-bonding interactions between the tweezerlike $[Fe(dapsox)(H_2O)_2]^+$ cation and the ClO_4^- anion have been observed,[3] this interaction, based on the performed electrochemical titrations, seems to be not strong enough to be observed in solution.

Lithium salts differ from tetrabutylammonium salts in that they increase the solubility of $[Fe(dapsox)(H_2O)_2]ClO_4$ and significantly shift the half-wave potential of [Fe(dapsox)-$(CH_3CN)_2]^{0/+}$ in CH_3CN. The addition of LiOTf, $LiClO_4$, or $LiBF_4$ to the electrolyte solution of $[Fe(dapsox)(CH_3CN)_2]^+$ (ionic strength of 0.1 M was kept constant) led to a progressive positive shift in the $E_{1/2}$ (one-wave behavior). The maximal shift in the half-wave potential is reached in the presence of an excess of guest species (Figure 1, Table S1). Cyclic and differential pulse voltammograms obtained during the electrochemical titrations of $[Fe(dapsox)(CH_3CN)_2]^+$ (Figure 2) show the presence of a single reversible

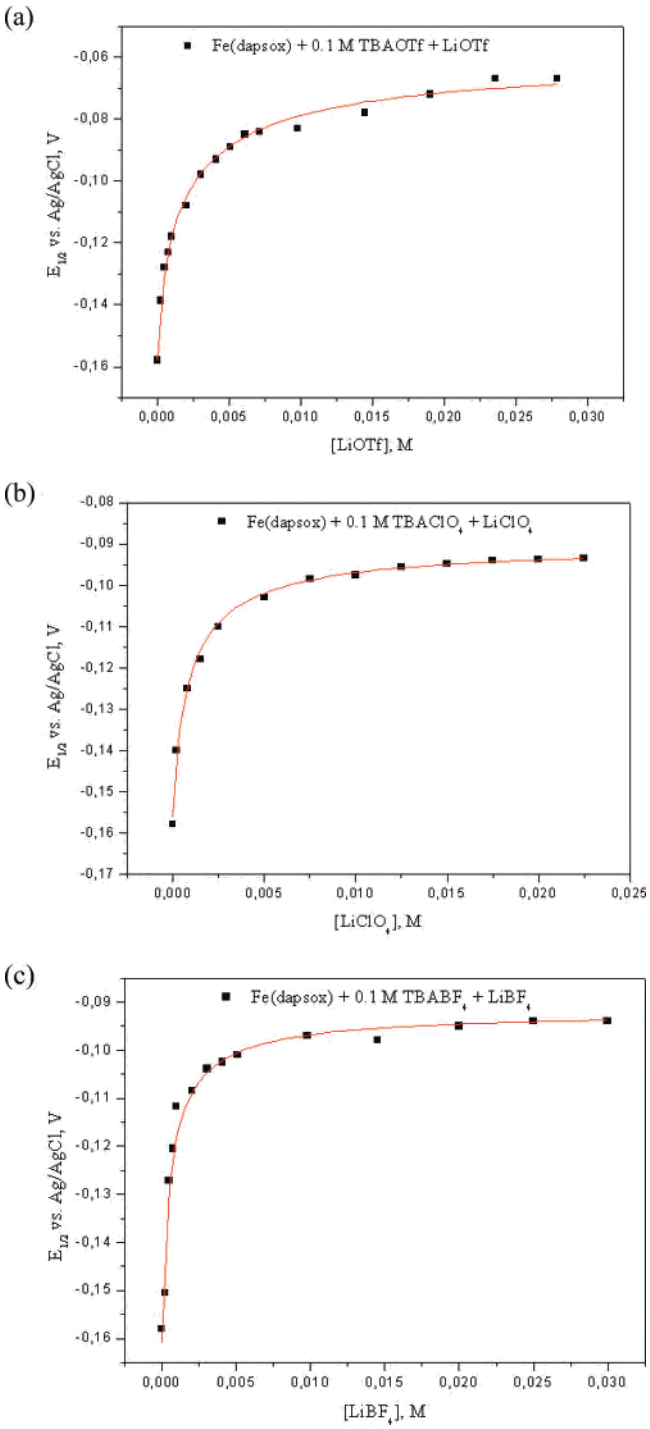

Figure 1. Plot of $E_{1/2}$ vs lithium salt concentration $[Li^+A^-]$ ($A = OTf^-$, ClO_4^-, BF_4^-); $[Fe(dapsox)(CH_3CN)_2]^+ = 1$ mM, 25 °C, $E_{1/2}$ vs Ag/AgCl electrode. The corresponding $NBu_4^+A^-$ salts (0.1 M) were used as supporting electrolytes. Solid curves represent nonlinear least-squares fitting of the data to eq 1.

(17) Butler, J. N. *Ionic Equilibrium: Solubility and pH Calculations*; Wiley: New York, 1998; p 474.
(18) Bernhardt, P. V.; Moore, E. G. *Aust. J. Chem.* **2003**, *56*, 239−258.

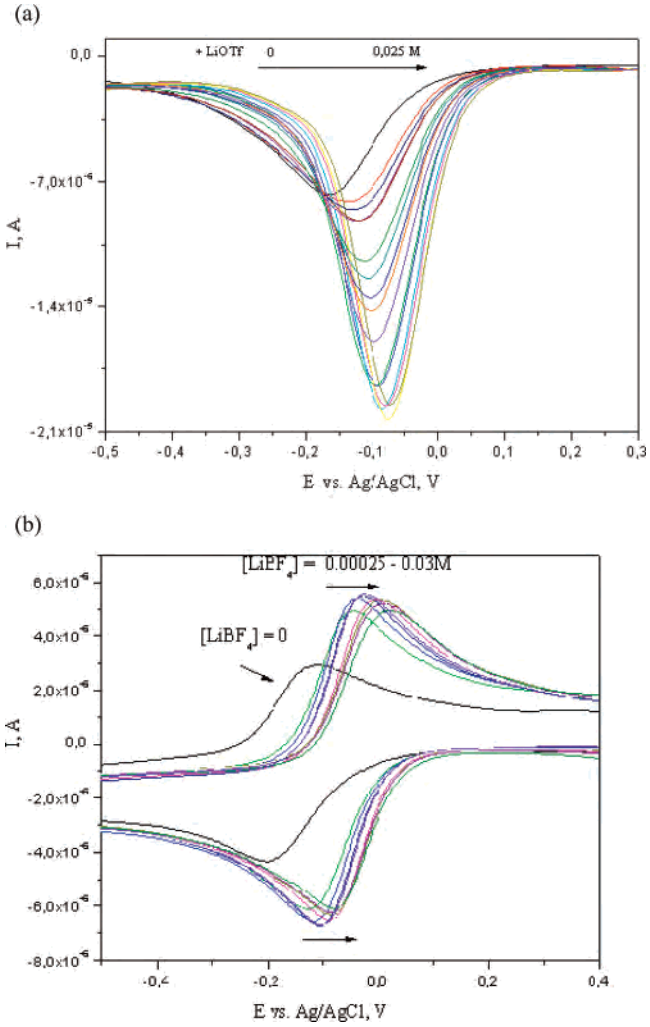

Figure 2. Typical electrochemical response of $[Fe(dapsox)(CH_3CN)_2]^{0/+}$ (1 mM) upon addition of increasing amounts of (a) LiOTf (differential pulse voltammograms) and (b) $LiBF_4$ (cyclic voltammograms) using corresponding NBu_4A salts (0.1 M) as electrolytes.

redox couple that shifts anodically with added lithium salt, indicating a weak binding.[18,19] The difference in diffusion coefficients of $[Fe(dapsox)(CH_3CN)_2]^+$ and its lithium salt adduct causes the difference in the current intensity observed in Figure 2.

The values of K^{II} are quite high ($\sim 10^4$) and are more than 1 order of magnitude greater than K^{III}, which is consistent with the observed positive shift of $E_{1/2}$, confirming that the reduced state of the receptor is stabilized upon complexation with lithium salts.[19−20] The K^{II} values are less sensitive to the nature of the counteranion than the K^{III} values, suggesting that the more prominent interaction with the anion exists in the case of the Fe(III) form of the complex. The somewhat higher apparent binding constants are observed for $LiBF_4$, where the strongest hydrogen-binding interactions between the anion and amide $-NH_2$ groups are to be expected.

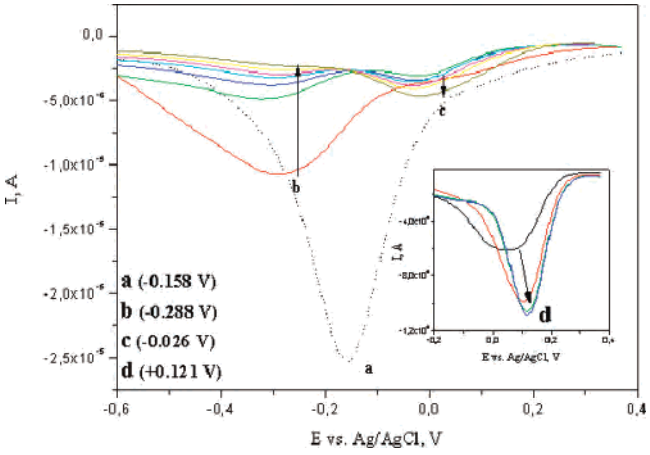

Figure 3. Differential pulse voltammograms representing electrochemical response of $[Fe(dapsox)(CH_3CN)_2]^{0/+}$ (1 mM) upon addition of increasing amounts of $LiPF_6$. The wave (a) is assigned to the $[Fe(dapsox)(CH_3CN)_2]^+$ in the absence of lithium salt. The waves (b) and (c) appear in acetonitrile solution of complex after addition of $LiPF_6$ (up to 0.0019 M). The wave (d) (inset) appears after further addition of $LiPF_6$ (0.0019−0.019 M).

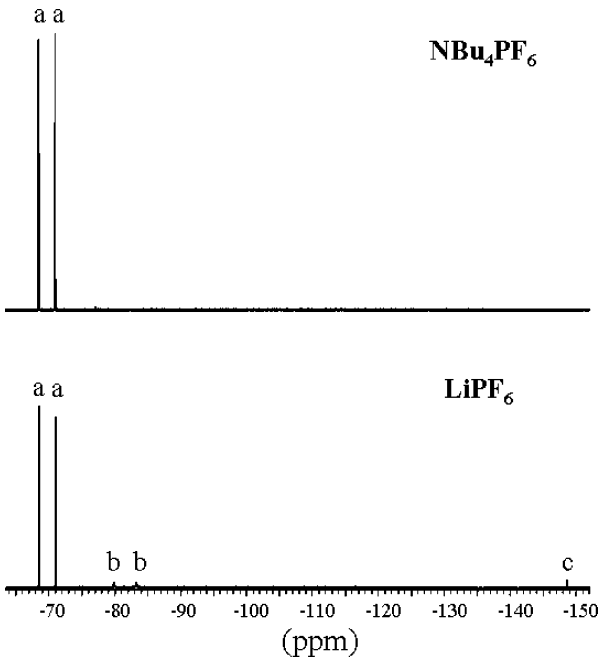

Figure 4. Typical ^{19}F NMR spectra of the CH_3CN solution, containing 0.2 M NBu_4PF_6 and 0.2 M $LiPF_6$. Signals (a) are assigned to PF_6^-. Signals (b) and (c) belong to $PO_2F_2^-$ and HF, respectively.

Consequently, a stronger anion binding results in the smaller shift of $E_{1/2}$, since, opposite from the Li^+ coordination, it increases the electron density around the metal center.

We have also performed the electrochemical titration with $NaClO_4$ in CH_3CN and with $LiBF_4$ in MeOH in order to test the cation and solvent variation effects (Table 1). In both cases, the K^{III} value was too small ($K^{III} < 10^{-1}$ M^{-1}) to be determined,[19b,c] showing that the interactions between the Fe(III) form of the complex and guest salts are very weak under those conditions. Comparison of the apparent binding constants K^{II} for $LiClO_4$ (4004 ± 402 M^{-1}) and $NaClO_4$ (2690 ± 400 M^{-1}) in CH_3CN (Table 1) leads to the conclusion that the complex exhibits modest Li^+ selectivity. The similar complexation selectivity was observed for several

(19) (a) Beer, P. D.; Gale, P. A.; Chen, G. Z. *J. Chem. Soc., Dalton Trans.* **1999**, 1897−1910. (b) Bernhardt, P. V.; Hayes, E. J. *Inorg. Chem.* **2002**, *41*, 2892−2902. (c) Bernhardt, P. V.; Hayes, E. J. *Inorg. Chem.* **2003**, *42*, 1371−1377.
(20) Moutet, J. C.; Saint-Aman, E.; Ungureanu, E. M.; Arion, V.; Gerbeleu, N.; Revenco, M. *Electrochim. Acta* **2001**, *46*, 2733−2740.

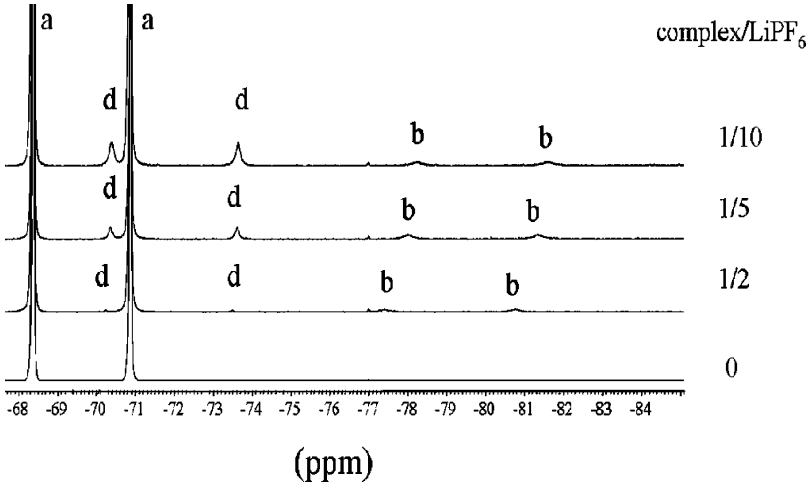

Figure 5. ^{19}F NMR spectra of the CH_3CN solutions at 25 °C, containing constant iron complex concentration (0.5 mM) and increasing concentrations of $LiPF_6$. Signals (a) and (b) are assigned to PF_6^- and [Fe(dapsox)(CH_3CN)(PO_2F_2)], respectively.

Table 1. Apparent Binding Constants for the Complexation of Li^+A^- Salts in CH_3CN by [Fe(dapsox)($CH_3CN)_2$] (K^{II}) and [Fe(dapsox)($CH_3CN)_2]^+$ (K^{III})

	solvent				
	CH_3CN				CH_3OH
apparent binding constants, M^{-1}	$Li^+CF_3SO_3^-$	$Li^+ClO_4^-$	$Li^+BF_4^-$	$Na^+ClO_4^-$	$Li^+BF_4^-$
K^{II} (electrochem)[a]	3754 ± 418	4004 ± 402	6616 ± 1812	2690 ± 400	2529 ± 301
K^{III} (electrochem)[a]	90 ± 11	309 ± 28	458 ± 102	<0.1[b]	<0.1[b]
K^{III} (^{7}Li NMR)[c]	203 ± 32				
K^{III} (kinetics)[d]	49 ± 10				
K^{III} (UV−vis spectra)[c]	165 ± 15				

[a] At 25 °C in 0.1 M NBu_4A. [b] Too small to determine. [c] At 25 °C with no supporting electrolyte. [d] At −15 °C in 0.2 M NBu_4A.

redox-active ferrocene crown ethers.[21] Polarity of the solvent also plays an important role.[7a,22] Therefore, in more polar MeOH, the interaction of the complex with $LiBF_4$ is weaker than in CH_3CN, resulting in the smaller apparent binding constants K^{II} and K^{III} (Table 1).

Solution Behavior in the Presence of $LiPF_6$. The electrochemical titration was also performed with $LiPF_6$. However, lithium-catalyzed hydrolysis of PF_6^- causes the appearance of additional fluorine-containing anionic species and HF,[23] which makes the solution chemistry more complex. Immediately upon addition of a small aliquot of 0.4 M $LiPF_6$ in CH_3CN (complex/Li^+ = 4:1 molar ratio), two new redox waves were observed (Figures 3 (DPV) and S3 (CV)): the intense one (b) with negatively shifted $E_{1/2}$ ($\Delta E_{1/2} = -130$ mV) and the lower intensity one (c) with positively shifted $E_{1/2}$ ($\Delta E_{1/2} = +132$ mV) relative to the original redox couple. The appearance of two redox waves and the negative shift in redox potential upon addition of lithium salt are unique observations. By increasing the lithium concentration, the intensity of wave (b) decreases and that of (c) increases (Figures 3 and S3).

To obtain more information about the species present in solution, the ^{19}F NMR measurements were performed. In the ^{19}F NMR spectrum of NBu_4PF_6 in acetonitrile, only one 1:1 doublet at $\delta_F = -69.8$, with the $^{31}P-^{19}F$ coupling constant $J(P,F) = 707$ Hz, is observed (Figure 4a), which is typical for PF_6^-.[23] However, the ^{19}F spectrum of $LiPF_6$ in CH_3CN consists of two doublets with chemical shifts (a) $\delta_F = -69.8$ [$J(P,F) = 707$ Hz] and (b) $\delta_F = -81.6$ [$J(P,F) = 959$ Hz], as well as the singlet (c) with $\delta_F = -148.6$ (Figure 4b). The major low-field doublet (a) is assigned to PF_6^-, whereas the doublet (b) is unambiguously assigned to the $PO_2F_2^-$ ion, which is the product of partial hydrolysis of PF_6^- in CH_3CN, accelerated by the presence of Li^+ ions in solution.[23] The singlet (c) is characteristic for HF, which is also consistent with the hydrolysis processes observed in the presence of Li^+.[23] When the complex (1 mM) was added to the solutions containing 0.1 M NBu_4PF_6 and different concentrations of $LiPF_6$, the downfield shift of the doublet (b) $\delta_F = -78.6$ [$J(P,F) = 946$ Hz] and the appearance of a new one (d), $\delta_F = -72.1$ [$J(P,F) = 920$ Hz] could be observed (Figure 5). The new doublet (d) corresponds to the PO_3F^{2-} anion.[23]

The observed anionic species ($A^- = PO_2F_2^-$ and PO_3F^{2-}) can act as the complexing agents,[24] resulting in the negatively shifted redox wave (b) (Figure 3). The positively shifted

(21) Plenio, H.; Diodone, R. *Inorg. Chem.* **1995**, *34*, 3964−3972.
(22) Severin, K. *Coord. Chem. Rev.* **2003**, *245*, 3−10.
(23) Plakhotnyk, A. V.; Ernst, L.; Schmutzler, R. *J. Fluorine Chem.* **2005**, *126*, 27−31.
(24) (a) Akbayeva, D. N.; Di Vaira, M.; Seniori Costantini, S.; Peruzzini, M.; Stoppioni, P. *Dalton Trans.* **2006**, 389−395. (b) Fernandez-Galan, R.; Manzano, B. R.; Otero, A.; Lanfranchi, M.; Pellinghelli, M. A. *Inorg. Chem.* **1994**, *33*, 2309−2312. (c) Fernandez-Galan, R.; Manzano, B. R.; Otero, A. *J. Organomet. Chem.* **1999**, *577*, 271−282. (d) White, C.; Thompson, S. J.; Maitlis, P. M. *J. Organomet. Chem.* **1977**, *134*, 319−325. (e) Wimmer, F. L.; Snow, M. R. *Aust. J. Chem.* **1978**, *31*, 267−278. (f) Mildvan, A. S.; Leigh, J. S.; Cohn, M. *Biochemistry* **1967**, *6*, 1805−1818. (g) Nowak, T. *Arch. Biochem. Biophys.* **1978**, *186*, 343−350.

wave (c) corresponds to the lithium salt adduct of [Fe(dapsox)-(CH_3CN)(A)]. This two-wave behavior can be interpreted in terms of the high stability constant of the lithium salt adduct.[25] The coordination of negatively charged A^-, affecting the overall charge of the complex, facilitates stronger Li^+ binding. Analogous to Scheme 2 and according to eq 2,[18,19a] the K^{II}/K^{III} quotient (the binding enhancement factor or the reaction coupling efficiency[19a]) is 52 600, suggesting the strong coupling between the lithium binding and iron reduction. It also shows that in the Fe(II) form the negatively charged [Fe(dapsox)(CH_3CN)(A)]$^-$ adduct binds Li^+ very efficiently.

$$\Delta E = \frac{RT}{F} \ln \frac{K^{II}}{K^{III}} \qquad (2)$$

At higher lithium concentrations, wave (b) vanishes whereas wave (c) becomes broader and starts to anodically shift further (wave (d) in Figures 3 and S3). These additional processes are most probably related to the further hydrolysis of PF_6^--related anionic species and increase in the HF concentration, which might result in protonation of the complex.

^{7}Li NMR Titrations. In order to better visualize the lithium ion binding to the seven-coordinate iron(III) complex, ^{7}Li NMR measurements were performed. Different from the electrochemical measurements, where the effects of host−guest interactions on the redox active iron center can be observed, ^{7}Li NMR titrations can demonstrate the complexation effect on the Li^+ cation itself. The NMR chemical shift titration has been widely used as a method for the determination of binding constants.[6a,26] The easily observed and sensitive ^{7}Li isotope has nuclear spin $I = 3/2$ and high abundance (95%), making it an attractive nucleus for NMR titrations.[27] In the case of host−guest complexation reactions, either the concentration of guest (^{7}Li nucleus) or of the host is varied and the resulting change in the chemical shift is followed. If the reaction is fast on the NMR time scale, only one shift will be observed, representing a concentration-weighted average of the shifts of free and bound species.

In the first set of measurements, the concentration of Li^+ (200 mM LiOTf) was kept constant. Three different probes with the iron complex concentration of 0.5, 1.0, and 1.5 mM were measured. It can be seen in Figure 6 that the lithium resonance peak broadens and shifts downfield (relative to the chemical shift of free Li^+ in CH_3CN with $\delta = 5.7$, see Figure 7), with an increase in [Fe(dapsox)($CH_3CN)_2$]$^+$ concentration. The downfield resonance shift is indicative of the complexation, implying that the solvation environment

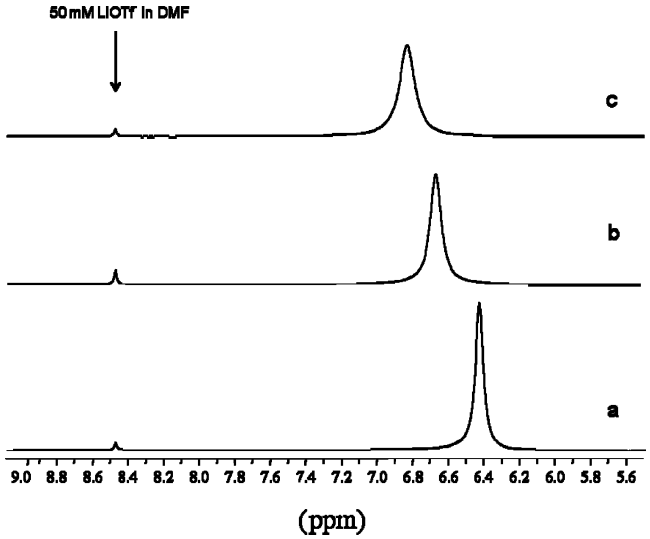

Figure 6. ^{7}Li NMR Spectra of LiOTf (0.2 M) solution in CH_3CN at 25 °C in the presence of (a) 0.5, (b) 1, and (c) 1.5 mM [Fe(dapsox)($CH_3CN)_2$]$^+$.

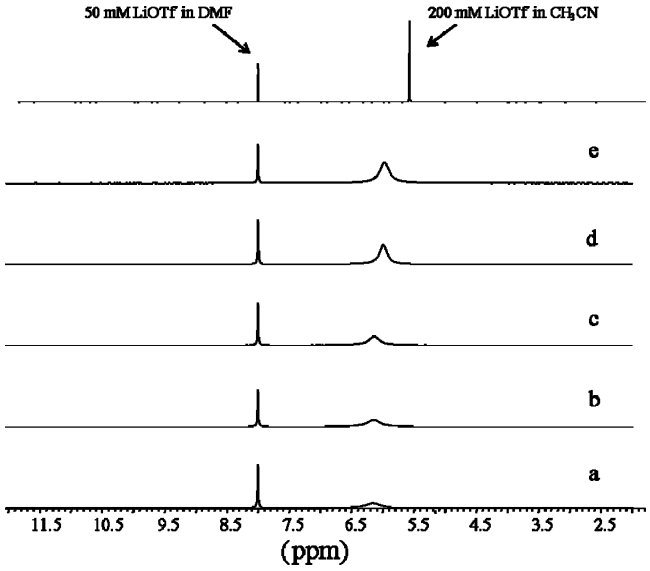

Figure 7. ^{7}Li NMR Spectra of (a) 5, (b) 15, (c) 25, (d) 35, and (e) 50 mM LiOTf in the presence of constant iron complex concentration (0.5 mM) in CH_3CN. Measurements were run at room temperature.

around the lithium cation is perturbed upon addition of the paramagnetic ($\mu_{eff} = 5.26\ \mu_B$)[3] receptor complex.

Another set of data was obtained by keeping the concentration of the iron complex constant (0.5 mM) and varying the concentration of Li^+ between 5 and 50 mM (Figure 7). Increase in the lithium salt concentration causes an upfield shift of the ^{7}Li resonance toward the position of free Li^+. This also provides qualitative evidence for the host−guest interaction.

In an attempt to quantitatively determine the apparent lithium binding constant, ^{7}Li NMR T_1 relaxation measurements were performed. The concentration of the seven-coordinate iron complex was held constant (0.5 mM), whereas the concentration of the lithium salts (LiOTf, $LiClO_4$, and $LiBF_4$) was varied between 5 and 50 mM (10−100-fold excess). The concentration ([Li^+] = 500 mM) was used in all cases to observe relaxation time at saturation

(25) Miller, S. R.; Gustowski, D. A.; Chen, Z. H.; Gokel, G. W.; Echegoyen, L.; Kaifer, A. E. *Anal. Chem.* **1988**, *60*, 2021−2024.
(26) (a) Masiker, M. C.; Mayne, C. L.; Eyring, E. M. *Magn. Reson. Chem.* **2006**, *44*, 220−229. (b) Popov, K.; Lajunen, L. H. J.; Popov, A.; Ronkkomaki, H.; Hannu-Kuure, M.; Vendilo, A. *Inorg. Chem. Comm.* **2002**, *5*, 223−225. (c) Shamsipur, M.; Madrakian, T. *J. Coord. Chem.* **2000**, *52*, 139−149.
(27) (a) Suzuki, M.; Koyama, H.; Noyori, R. *Tetrahedron* **2004**, *60*, 1571−1579. (b) Mueller, A.; Rehder, D.; Haupt, E. T. K.; Merca, A.; Boegge, H.; Schmidtmann, M.; Heinze-Brueckner, G. *Angew. Chem., Int. Ed.* **2004**, *43*, 4466−4470. (c) Reich, H. J.; Borst, J. P.; Dykstra, R. R.; Green, P. D. *J. Am. Chem. Soc.* **1993**, *115*, 8728−8741.

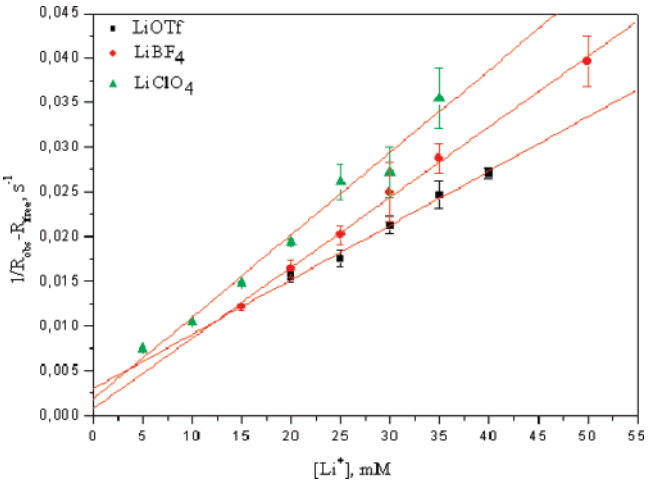

Figure 8. Representative James−Noggle plots for $[Fe(dapsox)(CH_3CN)_2]^+$ complex in the presence of (■) LiOTf, (red circles) $LiBF_4$, and (green triangles) $LiClO_4$. The *x* axis corresponds to the lithium salt concentrations used in the titrations of seven-coordinate iron complex, and the *y* axis represents $1/(R_{obs} - R_{free})$, where R_{obs} and R_{free} are the relaxation rates (or the reciprocals of the relaxation times) for the Li^+ nuclei of the observed sample ($T_{1(obs)}$) and with saturating Li^+ concentrations ($T_{1(free)}$), respectively (eq 3).

($T_{1(free)}$). Only one type of Li^+ binding site was assumed to be present, as well as monoexponential relaxation of the Li^+ nucleus (Figure S4) and fast exchange of Li^+ between free and bound states.[28] According to these assumptions, the apparent binding constants K^{III} were calculated from James−Noggle plots of ΔR^{-1} against $[Li^+]$ according to eq 3, using at least five ^7Li T_1 values,[13d,28,29] under the experimental conditions where $[Li^+] \gg [Fe]$

$$\Delta R^{-1} = (R_{obs} - R_{free})^{-1} = (K^{III})^{-1}\{[Fe](R_{bound} - R_{free})\}^{-1} + [Li^+]\{[Fe](R_{bound} - R_{free})\}^{-1} \quad (3)$$

$[Li^+]$ and [Fe] are the concentrations of Li^+ and iron complex, respectively. $R_{obs} = 1/T_{1(obs)}$, $R_{free} = 1/T_{1(free)}$, and $R_{bound} = 1/T_{1(bound)}$ are the relaxation rates (or the reciprocals of the relaxation times) for the Li^+ nuclei of the observed sample (R_{obs}), with saturating Li^+ concentrations (R_{free}(LiOTf) = 7.6 s^{-1}, $R_{free}(LiClO_4)$ = 5.6 s^{-1}, $R_{free}(LiBF_4)$ = 7.4 s^{-1}), or with Li^+ bound (R_{bound}), respectively (Table S2). This approach has the inherent approximation of using a binding model with a single type of Li^+ binding site, with a single K^{III} and R_{bound} value.

In all three cases, good linear plots of ΔR^{-1} vs $[Li^+]$ were obtained (Figure 8). By dividing the slopes of the linear fits (solid lines) in Figure 8 by the corresponding intercepts and multiplying the quotients by 1000, the values of the apparent binding constant K^{III} in M^{-1} could be derived (Table 1). However, the values obtained for the intercepts in the case of $LiClO_4$ and $LiBF_4$ are rather small with the high uncertainties and, consequently, could not be used for the quantification of K^{III}. In the case of LiOTf, the K^{III} binding constant was found to be 203 ± 68 M^{-1} (Table 1), which is somewhat higher than the corresponding value obtained from the electrochemical titration, general in agreement with the higher ionic strength of the solutions used in electrochemical experiments.

Spectrophotometric Determination of K^{III}. In an attempt to spectrophotometrically determine the K^{III} value, the $[Fe(dapsox)(CH_3CN)_2]^+$ complex was titrated with LiOTf at 25 °C. The absorbances at 460 nm vs [LiOTf] (inset in Figure S5) were fitted by applying eq 4

$$A_x = A_0 + \frac{(A_\infty - A_0)K^{III}[LiOTf]}{1 + K^{III}[LiOTf]} \quad (4)$$

The values of A_0 and A_∞ represent absorbance at 0% and 100% formation of complex, respectively, and A_x represents the absorbance at any given lithium triflate concentration. The observed spectral changes upon addition of LiOTf are not so prominent (Figure S5); however, the resulting apparent binding constant K^{III} = 165 ± 15 M^{-1} is in excellent agreement with the corresponding K^{III} value obtained by ^{7}-Li NMR measurements (Table 1), where in both experiments no additional supporting electrolyte was present in solution (experiments under the same ionic strength).

Reaction with SCN^- in CH_3CN. The kinetics of the reaction between $[Fe(dapsox)(CH_3CN)_2]^+$ complex and thiocyanate (SCN^-) in acetonitrile was studied under pseudo-first-order conditions (a large excess of SCN^-) at −15 °C and at constant ionic strength (I = 0.2 M), adjusted with NBu_4OTf and LiOTf (see below), respectively.

Spectral changes and corresponding kinetic traces (Figure 9) clearly showed two subsequent reaction steps over the whole SCN^- concentration range. Similar to what we found in aqueous, methanol, and ethanol solutions, the two reaction steps represent the substitution of two axially coordinated solvent molecules by SCN^-.[4b,c] Kinetic traces were fitted to a double-exponential function that resulted in k_{obs} values for the first and second reaction steps. Plots of k_{obs} vs $[SCN^-]$ (Figure 10) for both reaction steps at −15 °C in the presence of NBu_4OTf, as well as LiOTf, show a linear increase in k_{obs} with increasing $[SCN^-]$ over the whole concentration range, with more prominent intercepts in the case of the first reaction step. The dependence of k_{obs} on $[SCN^-]$ for both reactions can be expressed by eq 5, where k_1 and k_2 represent the rate constants for the forward reactions (from the slopes of the solid lines) and k_{-1} and k_{-2} represent the rate constants for the backward (from the intercepts) reactions in the presence of NBu_4OTf. For the reaction performed in the presence of LiOTf, an expression analogous to eq 5 can be applied for the first and second substitution, with the corresponding k_{1Li}, k_{2Li}, k_{-1Li}, and k_{-2Li} rate constants.

$$k_{obs(1,2)} = k_{1,2}[SCN^-] + k_{-1,-2} \quad (5)$$

From these values, the equilibrium constants $K_1^{SCN} = k_1/k_{-1}$ and $K_2^{SCN} = k_2/k_{-2}$ for the binding of the first and second SCN^- in the presence of NBu_4OTf and LiOTf can be

(28) Connors, K. A. *Binding Constants: The Measurements of Molecular Complex Stability*; Wiley: New York, 1987; p 350.
(29) James, T. L.; Noggle, J. H. *Proc. Natl. Acad. Sci. U.S.A.* **1969**, *62*, 644−649.

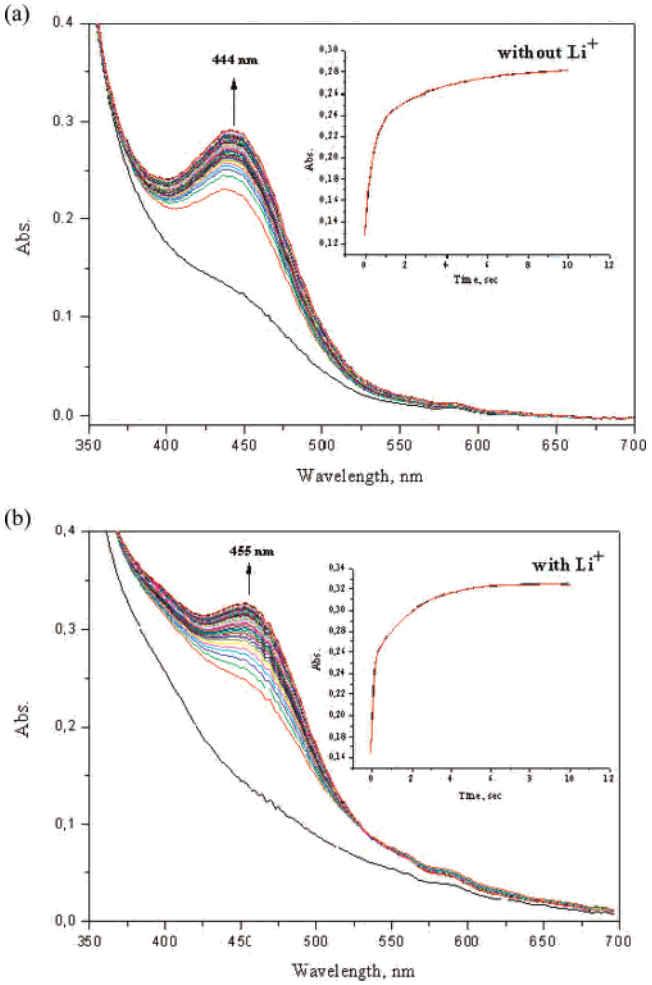

Figure 9. Spectral changes during the reaction of $[Fe(dapsox)(CH_3CN)_2]^+$ with NaSCN in the presence of (a) NBu_4OTf and (b) LiOTf ($[Fe(III)] = 5 \times 10^{-5}$ M, $[SCN^-] = 0.005$ M, $I = 0.2$ M, −15.0 °C). Inset: corresponding kinetic traces at 448 nm and double-exponential fits (solid lines).

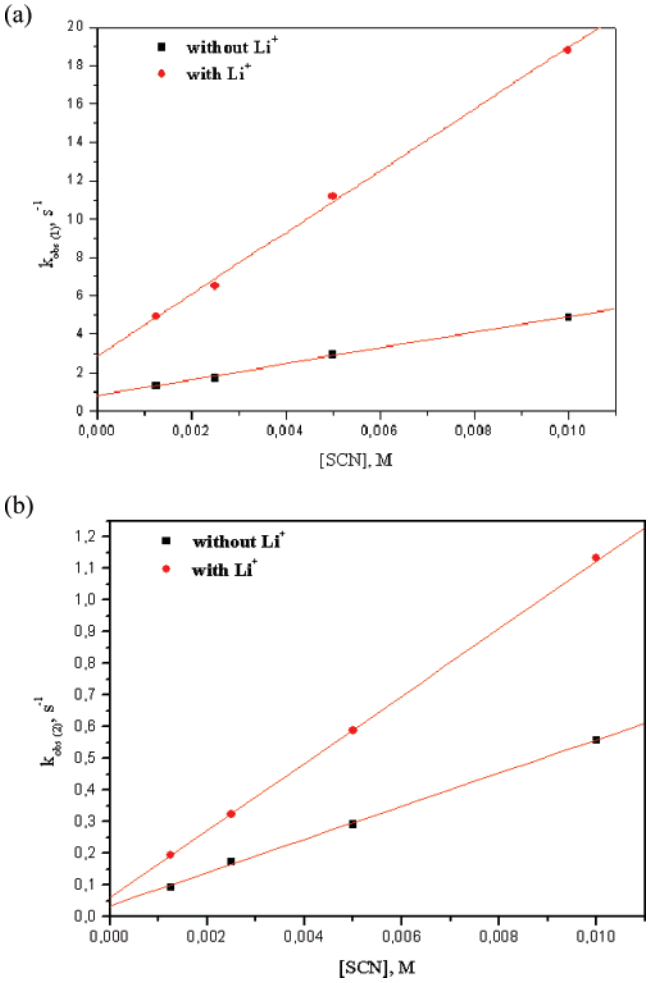

Figure 10. Plots of k_{obs} vs $[SCN^-]$ for the first (a) and second (b) reaction steps in the absence (■) and in the presence (red circles) of LiOTf. Experimental conditions: ($[Fe(III)] = 5 \times 10^{-5}$ M, $I = 0.2$ M, −15.0 °C).

calculated. The reaction scheme and corresponding rates and equilibrium constants are summarized in Scheme 3 and Table 2, respectively.

Equilibrium Studies for Binding of SCN^-. The equilibrium constants K_1^{SCN} and K_2^{SCN} were determined by spectrophotometric titrations of $[Fe(dapsox)(CH_3CN)_2]^+$ with NaSCN in CH_3CN solution at 25 °C. The spectral changes for the reactions with and without LiOTf ($I = 0.2$ M) are presented in Figure S6. For determination of equilibrium constants, the absorbances at 448 nm vs $[SCN^-]$ (insets in Figure S6) were fitted, in both cases, for the first and the second equilibrium together to eq 6.

$$A_x = \frac{A_0 + A_1K_1^{SCN}[SCN^-] + A_2K_1^{SCN}K_2^{SCN}[SCN^-]^2}{1 + K_1^{SCN}[SCN^-] + K_1^{SCN}K_2^{SCN}[SCN^-]^2} \quad (6)$$

The values of A_0 represent absorbance at 0% formation of complex, A_1 and A_2 ascribe absorbances of the $[Fe(dapsox)(CH_3CN)(NCS)]$ and $[Fe(dapsox)(NCS)_2]^-$ species, respectively, and A_x represents the absorbance at any given thiocyanate concentration $[SCN^-]$. The average values of K_1^{SCN} and K_2^{SCN} obtained by fitting titration curves at 448 nm according to eq 6, as well as independently over the 200−700 nm wavelength range, with Specfit/32 global analysis are summarized in Table 2.

Scheme 3

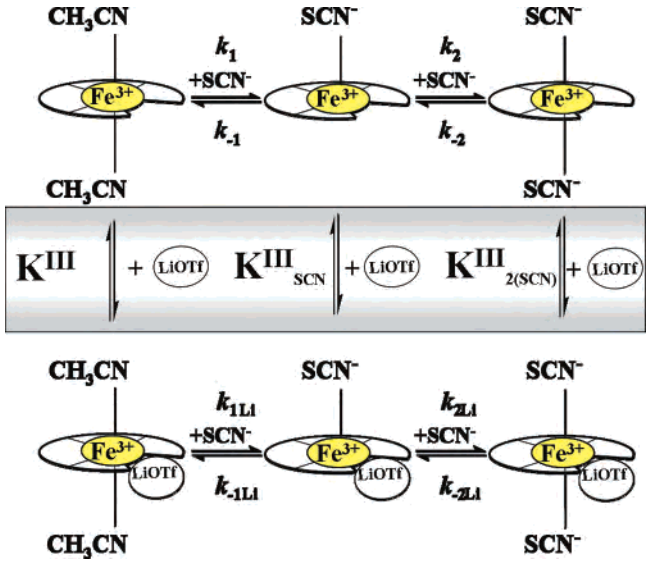

Table 2. Kinetic Results for the Reactions of NaSCN with $[Fe(dapsox)(CH_3CN)_2]^+$ at −15 °C and 0.2 M Ionic Strength in CH_3CN

	0.2 M (NBu_4OTf)		0.2 M (NBu_4OTf/LiOTf)
k_1, $M^{-1}\,s^{-1}$	411 ± 14	k_{1Li}, $M^{-1}\,s^{-1}$	1605 ± 51
k_{-1}, s^{-1}	0.79 ± 0.08	k_{-1Li}, s^{-1}	2.8 ± 0.3
K_1^{SCN}, M^{-1}	520 ± 56[a]		574 ± 64[a]
	237 ± 53[b]		727 ± 17[b]
$\Delta H_1^{\neq}$, kJ mol^{-1}	9 ± 2		
$\Delta S_1^{\neq}$, J $mol^{-1}\,K^{-1}$	−159 ± 6		
k_2, $M^{-1}\,s^{-1}$	52 ± 1	k_{2Li}, $M^{-1}\,s^{-1}$	106 ± 2
k_{-2}, s^{-1}	0.033 ± 0.007	k_{-2Li}, s^{-1}	0.056 ± 0.004
K_2^{SCN}, M^{-1}	1575 ± 336[a]		1893 ± 140[a]
	1326 ± 468[b]		1900 ± 210[b]
$\Delta H_2^{\neq}$, kJ mol^{-1}	4 ± 1		
$\Delta S_2^{\neq}$, J $mol^{-1}\,K^{-1}$	−195 ± 3		
K^{III}, M^{-1}			49 ± 10[c]
K_{SCN}^{III}, M^{-1}			152 ± 24[c]
$K_{2(SCN)}^{III}$, M^{-1}			775 ± 54[d]

[a] Calculated as $K_1^{SCN} = k_1/k_{-1}$, $K_2^{SCN} = k_2/k_{-2}$. [b] Results from nonlinear fitting of the spectrophotometric titration curves of $[Fe(dapsox)(CH_3CN)_2]$ and $\{[Fe(dapsox)(CH_3CN)_2]\cdot LiOTf\}$ with NaSCN at 25 °C (eq 6, Figure S6). [c] Determined by nonlinear fitting of saturation kinetic curves (eqs 7 and 8, Figure 11). [d] Results from nonlinear fitting of the spectrophotometric titration curves of $[Fe(dapsox)(NCS)_2]^-$ with LiOTf at 25 °C (eq 4, Figure S8).

Temperature-Dependent Kinetic Measurements. The electrochemical and NMR titrations of $[Fe(dapsox)(CH_3CN)_2]^+$ with LiOTf (see above) have shown that there is a host−guest interaction between the complex and lithium salt and that in the presence of 0.2 M LiOTf the predominant species in solution is the $\{[Fe(dapsox)(CH_3CN)_2]\cdot LiOTf\}^+$ adduct. At the same time, our kinetic and thermodynamic data for the reactions with SCN^- show (Figure 10 and Table 2) that in the presence of 0.2 M LiOTf both reaction steps proceed with higher rate constants (k_{1Li} and k_{2Li}) and the corresponding apparent binding constants ($K_1^{SCN}$and K_2^{SCN}) are also somewhat higher than in the case when instead of LiOTf, 0.2 M NBu_4OTf was present in solution. This clearly suggests that the $\{[Fe(dapsox)(CH_3CN)_2]\cdot LiOTf\}^+$ adduct has a higher reactivity toward the SCN^- anion and that its mono- and bis(thiocyanato) species have higher thermodynamic stability. To clarify mechanistically this phenomenon, we have performed the temperature-dependent kinetic measurements of the reaction of $[Fe(dapsox)(CH_3CN)_2]^+$ with SCN^- and 0.2 M NBu_4OTf as supporting electrolyte. Plots of k_{obs} vs $[SCN^-]$ for the first and second reaction steps as a function of temperature, and the corresponding Eyring plots are presented in Figures S7. The obtained activation parameters $\Delta H^{\neq}$ and $\Delta S^{\neq}$ are also included in Table 2. The very negative $\Delta S^{\neq}$ values suggest the associative nature of the rate-determining process for both substitution steps. In the case of previously studied reactions of $[Fe(dapsox)(S)_2]^+$ (S = H_2O, MeOH, EtOH, DMSO)[4b,c] with SCN^- in aqueous, alcoholic, and DMSO solutions, respectively, an associative interchange (I_a) mechanism (negative $\Delta S^{\neq}$ values) has been observed for the first substitution step. The second substitution step had the general dissociative character (D or I_d).[4b,c] However, $[Fe(dapsox)(CH_3CN)_2]^+$ shows a stronger associative character for both substitution steps, as well as the higher reactivity, with k_1 and k_2 (extrapolated to 25 °C) 2 and 1 order of magnitude higher than the corresponding values for the other studied $[Fe(dapsox)(S)_2]^+$ complexes, respectively.[4b,c] Increased reactivity and product stability in the case of the $\{[Fe(dapsox)(CH_3CN)_2]\cdot LiOTf\}^+$ adduct can also be explained in terms of an associative mechanism for the binding of SCN^-. The coordinated lithium cation close to the iron center decreases the electron density around the metal center and consequently increases its electrophility.

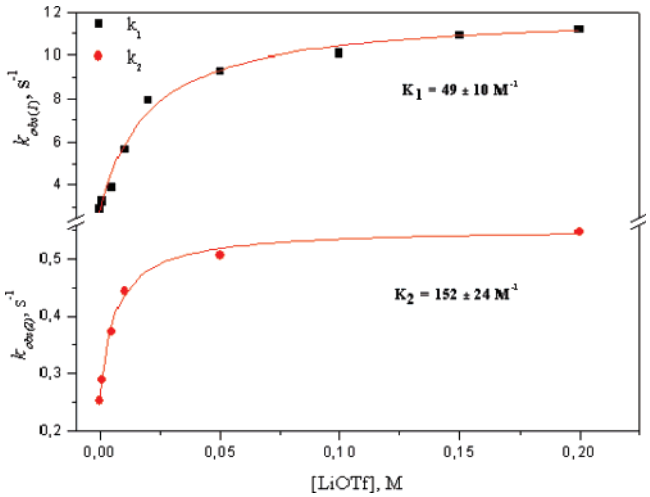

Figure 11. Dependences of $k_{obs(1)}$ and $k_{obs(2)}$ on the lithium concentration. Experimental conditions: ([Fe(III)] = 5 × 10^{-5} M, $[SCN^-]$ = 0.005 M, I = 0.2 M, −15.0 °C). Solid lines represent nonlinear fitting curves according to eqs 7 and 8.

Lithium-Dependent Kinetic Measurements. In order to better visualize the effect of the lithium cation on the kinetic behavior of our complex, we performed another set of measurements. The reaction was followed varying $[Li^+]$ and keeping $[SCN^-]$ and ionic strength constant. Dependences of $k_{obs(1)}$ and $k_{obs(2)}$ on the lithium concentration are depicted in Figure 11, showing an increase of the observed rate constants for both reaction steps with increasing lithium concentration. Significant curvatures are in agreement with the equilibrium between two different reactive species, $[Fe(dapsox)(CH_3CN)_2]^+$ ("lithium-free") and $\{[Fe(dapsox)(CH_3CN)_2]\cdot LiOTf\}^+$ ("lithium-bound") for the first, and [Fe(dapsox)(NCS)] ("lithium-free") and {[Fe(dapsox)(NCS)]·LiOTf} ("lithium-bound") for the second reaction step. According to Scheme 3, the first and second reaction

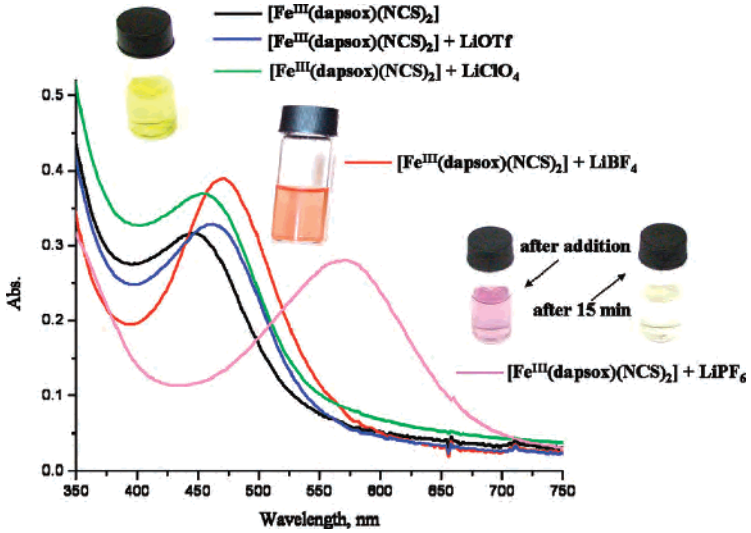

Figure 12. Spectra of the $[Fe(dapsox)(NCS)_2]^-$ solutions (5×10^{-5} M) measured after addition of different lithium salts (0.2 M) in CH_3CN and the change in color of corresponding product solutions.

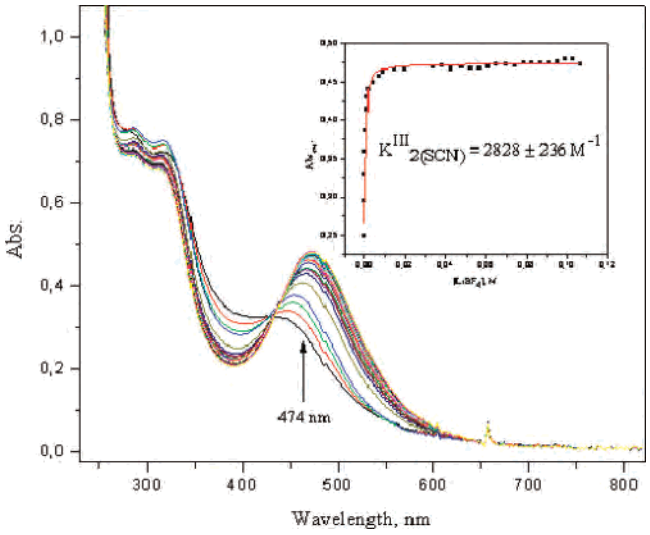

Figure 13. Spectral changes upon addition of $LiBF_4$ to the 5×10^{-5} M solution of $[Fe(dapsox)(NCS)_2]$. Inset: the change in absorbance at 474 nm plotted vs $[LiBF_4]$; solid line represents nonlinear fitting curve (according to eq 4).

steps can be expressed using the somewhat simplified rate laws:[30]

$$k_{obs(1)} = \frac{k_1 + k_{1Li}K^{III}[Li^+]}{1 + K^{III}[Li^+]}[SCN^-] + k_{-1Li} \qquad (7)$$

$$k_{obs(2)} = \frac{k_2 + k_{2Li}K^{III}_{SCN}[Li^+]}{1 + K^{III}_{SCN}[Li^+]}[SCN^-] + k_{-2Li} \qquad (8)$$

$k_{obs(1)}$ is the measured rate constant for the first reaction step, k_1, k_{1Li}, and k_{-1Li}[30] are the corresponding rate constants for the "lithium-free" and "lithium-bound" forms as reactive species (Scheme 3), and K^{III} is the equilibrium constant for the LiOTf binding to the $[Fe(dapsox)(CH_3CN)_2]^+$ complex. By analogy, $k_{obs(2)}$ is the measured rate constant for the second reaction step, k_2, k_{2Li}, and k_{-2Li}[30] are the corresponding rate constants for the "lithium-free" and "lithium-bound" forms as reactive species (Scheme 3), and K^{III}_{SCN} is the equilibrium constant for the LiOTf binding to the mono-(thiocyanato) [Fe(dapsox)(NCS)] adduct. Although the K^{III} and K^{III}_{SCN} values are not very high, suggesting that the binding of LiOTf to the iron complex in acetonitrile is not very efficient, the interaction is strong enough to affect the kinetic behavior. The K^{III} equilibrium constant corresponds to the constants obtained in electrochemical, and NMR experiments, respectively. The differences in the obtained values (Table 1) arise from the differences in the experimental conditions (temperature and ionic strength).

Spectrophotometric Observations. Different from the $[Fe(dapsox)(CH_3CN)_2]^+$ complex its bis(thiocyanato) $[Fe(dapsox)(NCS)_2]^-$ adduct with the strong charge-transfer band at 440 nm shows more prominent spectral changes upon addition of LiOTf, with a shift of the absorption maximum toward longer wavelengths (~460 nm) as the LiOTf concentration is increased (Figure S8). This allowed us to determine the apparent lithium binding constant to the $[Fe(dapsox)(NCS)_2]^-$ species ($K^{III}_{2(SCN)}$ in Table 2). The trend of $K^{III} < K^{III}_{SCN} < K^{III}_{2(SCN)}$ (Table 2) is consistent with the expectation that coordinated SCN^- will increase the nucleophilicity of the complex.

Although upon addition of LiOTf to the solution of $[Fe(dapsox)(NCS)_2]^-$ a shift in absorption maximum is observed, it does not cause a significant color change of the solution. Similar spectral changes are observed upon addition of $LiClO_4$. However, addition of $LiBF_4$ and $LiPF_6$ causes a significant change in the spectrum of $[Fe(dapsox)(NCS)_2]^-$ and, consequently, in the color of its solution. The spectral changes and the colors of the solutions, resulting from the addition of the same amount of different lithium salts (0.2 M) to $[Fe(dapsox)(NCS)_2]^-$ (5×10^{-5} M) in CH_3CN, are presented in Figure 12. In addition, $[Fe(dapsox)(NCS)_2]^-$ was

(30) Since the reverse rate constants are more prominent in the case of the "lithium bound" forms and the corresponding K^{III}_{SCN} and $K^{III}_{2(SCN)}$ values are relatively high, the terms for the overall reverse rate constants for the first and second reaction steps in eqs 7 and 8 can be reduced to k_{-1Li} and k_{-2Li}, respectively.

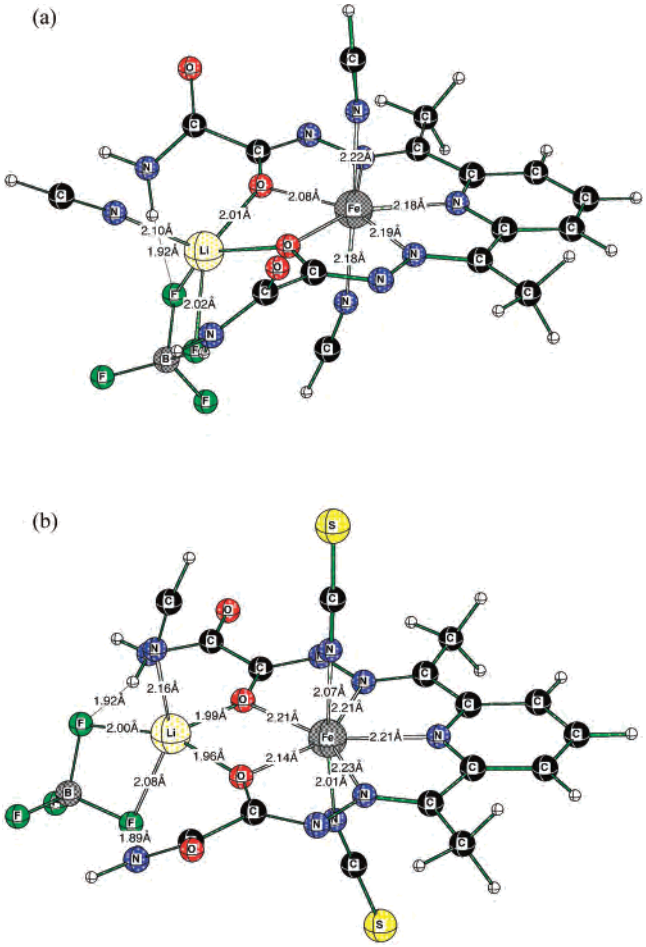

Figure 14. Calculated structures (B3LYP/LANL2DZp) of (a) $\{[Fe(dapsox)(CH_3CN)_2]\cdot LiBF_4\}^+$ and (b) $\{[Fe(dapsox)(NCS)_2]\cdot LiBF_4\}^-$.

titrated with $LiBF_4$ (Figure 13) and the corresponding $K^{III}_{2(SCN)}$ constant was determined to be 2828 ± 236 M^{-1}, showing a more prominent binding than in the case of LiOTf (Table 2).

The product solutions in the case of LiOTf, $LiClO_4$, and $LiBF_4$ are stable, whereas the solution with $LiPF_6$ becomes colorless within 15 min. Interestingly, lower $[LiPF_6]$ (up to 0.004 M) causes similar spectral changes as those observed with 0.2 M $LiBF_4$ (Figures 12 and S9), but further addition of $LiPF_6$ leads to the absorbance decrease and shift of the maximum to 570 nm (Figure S9). The resulting violet solution bleaches in a short time. The violet color and the absorbance at 570 nm are typical for the Fe(II)−thiocyanato species, which is formed in the redox reaction between Fe(III) and SCN^- in acetonitrile, and dissociates to Fe(II) and thiocyanogen $(SCN)_2$, resulting in a colorless solution.[31] Such complex chemistry suggests that in the presence of $LiPF_6$ and high $[SCN^-]$, dechelation of the iron(III) $[Fe(dapsox)(NCS)_2]^-$ complex takes place, followed by the above-mentioned redox processes.

DFT Calculations. Since the attempts to crystallize the seven-coordinate Fe(III) complex with bound lithium salt were not successful, we performed DFT calculations to provide insight into the structural characteristics of the $\{[Fe(dapsox)(CH_3CN)_2]\cdot LiBF_4\}^+$ adduct, with the strongest interaction between the iron complex and lithium salt (Table 1) and its bis(thiocyanato) $\{[Fe(dapsox)(NCS)_2]\cdot LiBF_4\}^-$ form (Figure 13). Instead of acetonitrile, hydrogen cyanide was used as a working model for the calculations. The obtained structures are shown in Figure 14.

In the calculated structures, the BF_4^- anion interacts with the seven-coordinate iron complex by forming hydrogen bonds between the fluoride atoms and two hydrogen atoms of the pendant amide groups of the $dapsox^{2-}$ ligand. The two amide parts of the ligand are held in a preorganized arrangement by coordination of the α-oxyazine oxygen atoms to the iron center and, together with the bound anion, define a pocket of suitable size to host the Li^+ cation. The Li^+ cation binds to the negatively charged α-oxyazine oxygen atoms, solvent molecule, and the two fluoride atoms of BF_4^- which closes the tweezerlike pocket.

The Fe−N bond lengths in the equatorial plane are in excellent agreement with that found in the crystal structure of $[Fe(dapsox)(H_2O)_2]ClO_4$.[3] As expected, upon Li^+ coordination, the Fe−O^- bonds become longer (2.08 Å, Figure 14a) than those observed in the crystal structure of $[Fe(dapsox)(H_2O)_2]ClO_4$ (2.046(3) and 2.066(3) Å) due to the partial neutralization of the negative charge of the α-oxyazine oxygen donor atoms. Negative charge of the bridged α-oxyazine oxygen atoms results in somewhat shorter Li−O^- bonds (2.01 Å, Figure 14a) than the ones calculated for $[Li(H_2O)_5]^+$ (average d(Li−O) = 2.07 Å).[32]

The coordination of two SCN^- to the iron center causes elongation of the equatorial Fe−ligand bonds, whereas the elongation of Fe−O^- bonds is more prominent than that of the Fe−N bonds. At the same time, an increase in the electron density upon SCN^- coordination results in somewhat shorter Li−O bonds (Figure 14b). This is in agreement with the higher apparent LiOTf binding constant for $[Fe(dapsox)(NCS)_2]^-$, $K^{III}_{2SCN,}$ than for $[Fe(dapsox)(CH_3CN)_2]^+$, K^{III} (Table 2). The N−H···F hydrogen bonds are not affected by the changes in the coordination sphere of the more distant iron center.

Conclusion

In the present paper, we have shown by electrochemical, NMR, kinetic, thermodynamic, spectrophotometric, and DFT studies that the seven-coordinate $[Fe(dapsox)(CH_3CN)_2]^+$ complex behaves as a ditopic receptor for lithium salts in acetonitrile. The observed apparent binding constants increase in the order LiOTf < $LiClO_4$ < $LiBF_4$. In the case of $LiPF_6$, the solution chemistry is more complex due to the lithium-catalyzed PF_6^- hydrolysis processes. However, the electrochemical measurements with $LiPF_6$ show that the coordination of anionic species (in that case $PO_2F_2^-$ or PO_3F^{2-}) to the iron center strongly increases the interactions between the complex and lithium salt and the coupling between the lithium binding and iron reduction. From the kinetic and thermodynamic studies of the reaction between [Fe(dapsox)-

(31) Kratochvil, B.; Long, R. *Anal. Chem.* **1970**, *42*, 43−46.

(32) Puchta, R.; Galle, M.; van Eikema Hommes, N.; Pasgreta, E.; van Eldik, R. *Inorg. Chem.* **2004**, *43*, 8227−8229.

$(CH_3CN)_2]^+$ and SCN^- in the presence of NBu_4OTf and LiOTf, respectively, it has also been concluded that the increase in the electron density around the iron center upon anion coordination facilitates lithium binding. These experiments show that in nonaqueous media lithium salts cannot be simply used as supporting electrolytes, since they can affect the kinetic behavior of the studied complex. Mechanistic studies have revealed that the $[Fe(dapsox)(CH_3CN)_2]^+$ complex and its mono(thiocyanato) adduct undergo substitution processes according to an associative (A) mechanism. This can be interpreted in terms of the poor donor ability of CH_3CN, where the $Fe-NCCH_3$ bonds are so labilized that the rate-determining step has almost only $Fe-NCS^-$ bond making character. The higher reactivity of the lithium adduct of the complex also speaks in favor of an associative character of the rate-determining step in the substitution mechanism.

In conclusion, the seven-coordinate $[Fe(dapsox)(CH_3CN)_2]^+$ complex, in its Fe(III), Fe(II), and anion-substituted forms, having a shape of "charged tweezers", is able to intimately associate with the lithium salts by means of shape recognition, hydrogen-bond complementarity, and charge assistance. This, together with the possibility for simple synthetic variations, which our ligand system offers, make these types of mononuclear complexes promising structural motifs for designing efficient lithium salt receptors that can meet the requirements in terms of different applications.

Acknowledgment. The authors gratefully acknowledge fruitful discussions with Prof. Rudi van Eldik, Prof. Klaus Koch (University of Stellenbosch, South Africa), and Joachim Maigut and the financial support from the Deutsche Forschungsgemeinschaft through SFB 583 "Redox-active Metal Complexes".

Supporting Information Available: Electrochemical data; ^{7}-Li NMR T_1 and R values; cyclic voltammograms of Fc/Fc^+ couple in CH_3CN in the presence of different lithium salts; the half-wave potentials of $[Fe(dapsox)(CH_3CN)_2]^{0/+}$ vs different anion concentrations; cyclic voltammograms of $[Fe(dapsox)(CH_3CN)_2]^{0/+}$ in the presence of $LiPF_6$; a monoexponential relaxation of the Li^+ nucleus, obtained by using the inversion recovery pulse sequence; different spectrophotometric titration data; and temperature-dependent kinetic measurements. This material is available free of charge via the Internet at http://pubs.acs.org.

IC7005056